Published in final edited form as:
J Phys Chem B. 2009 July 23; 113(29): 9901–9908. doi:10.1021/jp8075832.

Formation of Carotenoid Neutral Radicals in Photosystem II

Yunlong Gao[‡], **Katherine E. Shinopoulos**[‡], **Cara A. Tracewell**[‡,§], **A. Ligia Focsan**[‖], **Gary W. Brudvig**[*,‡], and **Lowell D. Kispert**[*,‖]
Department of Chemistry, Yale University, P.O. Box 208107, New Haven, Connecticut 06520-8107, and Department of Chemistry, The University of Alabama, P.O. Box 870336, Tuscaloosa, AL 35487

Abstract

β-carotene radicals produced in the hexagonal pores of the molecular sieve Cu(II)-MCM-41 were studied by ENDOR and visible/near IR spectroscopies. ENDOR studies showed that neutral radicals of β-carotene were produced in humid air under ambient fluorescent light. The maximum absorption wavelengths of the neutral radicals were measured and were additionally predicted by using time-dependent density functional theory (TD-DFT) calculations. An absorption peak at 750 nm, assigned to the neutral radical with a proton loss from the 4(4') position of the β-carotene radical cation in Cu (II)-MCM-41, was also observed in photosystem II (PS II) samples using near-IR spectroscopy after illumination at 20 K. This peak was previously unassigned in PS II samples. The intensity of the absorption peak at 750 nm relative to the absorption of chlorophyll radical cations and β-carotene radical cations increased with increasing pH of the PS II sample, providing further evidence that the absorption peak is due to the deprotonation of the β-carotene radical cation. Based on a consideration of possible proton acceptors that are adjacent to β-carotene molecules in photosystem II, as modeled in the X-ray crystal structure of Guskov et al. *Nat. Struct. Mol. Biol.* **2009**, *16*, 334-342, an electron-transfer pathway from a β-carotene molecule with an adjacent proton acceptor to $P680^{\bullet+}$ is proposed.

Introduction

Carotenoids play many roles in photosynthetic organisms, including both light harvesting and photoprotection. Carotenoids absorb light in a region of the solar spectrum that chlorophylls do not harvest efficiently and are also able to quench chlorophyll triplet states, preventing photodamage or formation of singlet oxygen.[1] Recently, the β-carotene (Car) radical cation ($Car^{\bullet+}$) has received more interest due to its involvement in the secondary electron-transfer reactions of photosystem II (PS II). Uniquely in PS II, which is capable of oxidizing water to dioxygen, Car[2–7] and chlorophyll (Chl)[8,9] oxidation occurs under circumstances when electron donation to the primary electron-donor chlorophyll of PS II ($P680^{\bullet+}$) by the oxygen-evolving complex is blocked or slowed. Two different $Car^{\bullet+}$ species[6,7] and up to five different $Chl^{\bullet+}$ species[9] have been identified. The secondary electron-transfer reactions have been proposed to protect PS II against uncontrolled oxidative reactions of the high-potential species $P680^{\bullet+}$ when the primary electron-transfer pathway is inhibited.[10]

UV/visible absorption,[11] resonance Raman,[12] isomerization,[13,14] and Stark effect[15] studies of several carotenoid radical cations have been reported, helping to understand the biological role

[*]To whom correspondence should be addressed. Gary Brudvig: Phone: (203) 432-5202. Fax: (203) 432-6144. gary.brudvig@yale.edu.. [*]Lowell Kispert: Phone: (205) 348-7134. Fax: (205) 348-9104. lkispert@bama.ua.edu..
[‡]Yale University
[§]Current address: Department of Chemical Engineering, California Institute of Technology, Pasadena, CA 91125
[‖]The University of Alabama

Supporting Information Hyperfine coupling constants used in the ENDOR simulations calculated at the B3LYP/TZP(Ahlrichs) // B3LYP/6-31G** level. This material is available free of charge via the Internet at http://pubs.acs.org.

of $Car^{\bullet+}$. A recent study showed that $Car^{\bullet+}$ with a pKa of 4–7[16] was deprotonated under photo-irradiation in a silica-alumina solid support environment.[17] The proton was lost from a methyl group of $Car^{\bullet+}$ located at either the 5(5'), 9(9') or 13(13') position (Chart 1). This led to the formation of a neutral π-radical denoted as $\#Car^{\bullet}(5)$ (proton loss from the 5-methyl group), $\#Car^{\bullet}(9)$ (proton loss from the 9-methyl group) or $\#Car^{\bullet}(13)$ (proton loss from the 13-methyl group).

More recent studies using the molecular sieve Cu(II)-MCM-41[18] or silica-alumina[19] as solid support under UV irradiation showed that loss of a proton from the 4(4') position of some carotenoid radical cations (including $Car^{\bullet+}$[18] and the zeaxanthin$^{\bullet+}$,[19] among others) produces the most stable neutral radical denoted as $\#Car^{\bullet}(4)$. However, proton loss from the 4(4') position of some other naturally-occurring carotenoids is not favorable, such as violaxanthin, which contains two epoxide groups at the 5(5')-6(6') positions.[18,19] Under high light stress, zeaxanthin replaces violaxanthin in the PS II light-harvesting complexes (LHC II) through the xanthophyll cycle. The deprotonation of the zeaxanthin radical cation at the 4(4') position and formation of the neutral radical has been hypothesized[19] to play a role in the xanthophyll cycle as the mechanism of quenching the chlorophyll singlet or/and triplet states in the LHC II of pea and spinach plants. Based on their crystal structures,[20,21] the locations of the 4(4') positions of the zeaxanthin radical cation, close to the aqueous stromal and lumenal surfaces, are conducive to deprotonation. It is known from electrochemical measurements that deprotonation of carotenoid radical cations is facilitated by proton acceptors such as water; however, the deprotonation of the violaxanthin radical cation at the 4(4') positions is prevented by its epoxide groups.[19]

In the current study, the radicals of Car produced in the hexagonal pores of the molecular sieve Cu(II)-MCM-41 were characterized by ENDOR spectroscopy, visible/near-IR spectroscopy and DFT calculations. The molecular sieve Cu(II)-MCM-41 has been used previously as a matrix to stabilize the carotenoid radical intermediates formed upon catalytic- or photo-oxidation via electron transfer to the silicate matrix.[22,23] Electron transfer is greatly enhanced in metal-substituted MCM-41 matrices where the carotenoid can interact with an electron acceptor, generally a transition metal. The proximity of Car to the electron acceptor increases the photoyield of $Car^{\bullet+}$. In Cu(II)-MCM-41 prepared as in [reference 22], the distance between Cu^{2+} and the carotenoid in the Cu^{2+}-Car complex is short (~ 3 Å), thus favoring light-driven electron transfer from Car to Cu^{2+} and also permitting the thermal back electron transfer from Cu^{+} to $Car^{\bullet+}$.[22] It was observed that an absorption peak at 750 nm, which is assigned to $\#Car^{\bullet}(4)$ in Cu(II)-MCM-41, is also present in PS II samples that have been illuminated at low temperatures.[7] Previously, this peak was unassigned in PS II samples, and its wavelength is anomalous for a peak arising from $Car^{\bullet+}$ or $Chl^{\bullet+}$. It was observed that the intensity of the absorption peak at 750 nm increases with an increase of the irradiation time at cryogenic temperatures, as a charge separation involving oxidation of one of the secondary electron donors and reduction of Q_A is produced, and decreases as the charge separation decays by recombination, indicating that the species with the absorption peak at 750 nm is associated with one of the secondary electron donors in PS II. Herein, it is proposed that the absorption peak at 750 nm is due to the deprotonated neutral radical of β-carotene, $\#Car^{\bullet}(4)$. This suggestion is further supported by the observation that the intensity of the absorption peak at 750 nm relative to that of the β-carotene radical cation peak at 990 nm increases with increasing pH of the PS II sample.

Deprotonation of a specific $Car^{\bullet+}$ molecule would be facilitated by proton movement in the vicinity, perhaps including an adjacent proton-accepting amino-acid residue, and would require an electron-transfer pathway from the specific Car molecule to $P680^{\bullet+}$, an unexamined aspect of the secondary electron-transfer pathway in PS II. The possible proton-acceptor sites and electron-transfer pathways were investigated using the X-ray crystal structure of PS II from

the cyanobacteria *Thermosynechococcus elongatus*,[24] providing a mechanism for the formation of #Car$^{\bullet}$ in PS II and an explanation for the previously unassigned near-IR peak at 750 nm.

Experimental Methods

Chemicals

β-carotene was purchased from Fluka and purified by extraction with benzene and precipitation with methanol. Anhydrous dichloromethane (CH_2Cl_2) was purchased from Aldrich.

Preparation of Carotenoid Radicals in Cu(II)-MCM-41

Cu(II)-MCM-41 was synthesized as previous reported.[22] The uniform hexagonal pores (40 Å) of MCM-41, obtained by a templating mechanism similar to that reported by Beck et al.,[25] permit incorporation of carotenoids that can transfer electrons to the silicate matrix. Fresh Cu (II)-MCM-41 samples were dried at 110 °C for 3 hours. 100 mg of the dried sample was activated in an oven at 200 °C for 24 h and removed from the oven. Before the activated Cu (II)-MCM-41 sample cooled down below 100 °C, and before adsorbed water deactivated the sample, it was used immediately or transferred into an inert gas dry box where it was stored to prevent the accumulation of water that would deactivate the sample.

The preparation of samples of Cu(II)-MCM-41 powder containing only Car$^{\bullet+}$, only #Car$^{\bullet}$, or a mixture of Car$^{\bullet+}$ and #Car$^{\bullet}$ requires different procedures. To prepare a sample containing only Car$^{\bullet+}$, it has been shown that moisture and light must be absent from the activated Cu(II)-MCM-41 powder.[26] In the presence of moisture, the Cu(II)-MCM-41 becomes deactivated and Car$^{\bullet+}$ is not formed.[22] However, in the absence of water, exposure of the activated Cu(II)-MCM-41 powder sample containing carotenoids to light results in a mixture of Car$^{\bullet+}$ and #Car$^{\bullet}$ radicals.[17–19,27,28] It is also known that #Car$^{\bullet}$ can be formed from Car$^{\bullet+}$ due to the fact that water functions as the base to deprotonate Car$^{\bullet+}$. For instance, when moisture was added to a carotenoid solution during CV measurements, an irreversible CV wave occurred.[29] This was a result of the hydrolysis of Car$^{\bullet+}$ and of Car^{2+} formation during the oxidation cycle, and resulted in the subsequent appearance of CV waves due to #Car$^{\bullet}$ formation during the reduction cycle.[30,31] Therefore, the preparation of samples containing only #Car$^{\bullet}$ was accomplished by first generating Car$^{\bullet+}$ and then adding excess water vapor to deprotonate Car$^{\bullet+}$.

To prepare the Cu(II)-MCM-41 samples containing only #Car$^{\bullet}$, 4 mL of an anhydrous solution of 0.1 M Car in CH_2Cl_2 was added to the activated Cu(II)-MCM-41 powder sample, generating Car$^{\bullet+}$ by electron transfer. The mixture of activated Cu(II)-MCM-41 and Car$^{\bullet+}$ was then transferred to a beaker on the bench top and stirred under fluorescent light for about 5 minutes in humid air to evaporate the solvent. The color of the mixture changed from light yellow to blue green, indicating the hydrolysis of all the Car$^{\bullet+}$ and subsequent formation of #Car$^{\bullet}$. The residual solvent was removed under vacuum.

For visible/near-IR spectroscopic measurements, 20 mg of Car in Cu(II)-MCM-41 prepared as above was ground to a very fine powder and made into a large pellet using a pellet press (Parr Instrument Company, Moline, IL U. S. A.). Another 20 mg of activated Cu(II)-MCM-41 without the carotenoids was also ground to very fine powder and a pellet was prepared as above. This pellet was used as the background sample in the optical measurement.

For pulsed ENDOR measurements, samples of carotenoids in Cu(II)-MCM-41 were prepared in the usual way for EPR measurements[22] using a dry box and a vacuum line. Solutions of carotenoids were prepared in an inert gas dry box using anhydrous CH_2Cl_2. In a dry box, the solution was added to an EPR tube containing activated Cu(II)-MCM-41 and transferred to a vacuum line where the solvent was removed. In the absence of UV photolysis, the activated

Cu(II)-MCM-41 generated $Car^{\bullet+}$ by electron transfer, forming Cu^{+}. However, if the EPR samples were UV irradiated,[11,13,16] $\#Car^{\bullet}$ were formed in addition to $Car^{\bullet+}$. To gain the highest signal to noise required for ENDOR measurements, the sealed EPR sample was irradiated with a 200 W Xe lamp at 77 K to maximize the yield of carotenoid radicals.

Photosystem II Sample Preparation and Treatment

The procedures for preparation and treatment of *Synechocystis* PCC 6803 PS II core complexes, and for near-IR absorption measurements of PS II samples, are described in reference 7.

Calculations

The B3LYP functional included in the Gaussian 03 package[32] was used in all DFT calculations. Geometry optimization of $Car^{\bullet+}$ and $\#Car^{\bullet}$ was carried out using the 6-31G** basis set without symmetry constraints, as reported in recent studies.[17–19] The maximum absorption wavelengths (λ) and oscillator strengths (f) of the radicals were calculated by the TD-DFT method using the 6-31G* basis set. Three excited states were used for the $\#Car^{\bullet}$ and $Car^{\bullet+}$ calculations, and six excited states were used for the Car dication (Car^{2+}) calculation. Solvent effects were not included due to the size of the calculation, but could be estimated using the difference between the experimentally-observed and DFT-calculated λ. For $Car^{\bullet+}$, the difference between the maximum observed experimentally in PS II (982 nm) and calculated in the gas phase with the TD-DFT method (829 nm) was 0.24 eV, a value similar to typical errors of 0.2 – 0.5 eV in DFT calculations.[33–36] The difference for $\#Car^{\bullet}$(4) was 0.4 eV. Scaling by these differences takes into account both errors in the DFT calculations and solvent effects.

Simulation of Mims ENDOR spectra

Pulsed ENDOR simulations were performed using the SimBud/SpecLab programs.[37] SimBud contains various default EPR and ENDOR parameters as input, which have been replaced with experimental and calculated values in the current study. In order to simulate the Mims ENDOR spectra, the experimental parameters for microwave frequency (GHz), g tensors, magnetic field (G), initial and final ENDOR frequency (MHz), number of data points in the ENDOR file, and τ (μs) were used. A line width of 1 MHz was used for the simulations. In order to simulate individual spectra for each coupling of a radical, two of the DFT-calculated dipolar components (T_{11},T_{22},T_{33}) of a traceless tensor (MHz) and the DFT-calculated isotropic coupling (Fermi contact) (MHz) were used. SpecLab was then used to process the data, summing the individual spectra due to each isotropic coupling to give the total Mims ENDOR spectrum of the radical.

All calculated couplings, both isotropic and anisotropic, were obtained using the B3LYP/TZP (Ahlrichs) // B3LYP/6-31G** method, which gives values within 0.5 MHz of the experimentally-deduced couplings.[17] The DFT-calculated anisotropic coupling constants[27] are listed in the Supporting Information and were used in the simulations without change.

Instrumentation

Visible/near-IR measurements of carotenoid radicals in Cu(II)-MCM-41 were carried out using a Varian CARY 50 spectrometer (Varian Australia Pty. Ltd.). Visible/near-IR measurements on PS II samples were carried out using a Perkin-Elmer Lambda 20 spectrometer with an Oxford Instruments Optistat liquid helium cryostat. Pulsed ENDOR experiments were carried out with a Bruker ELEXSYS E-680 W/X FT/CW PULSE X-BAND EPR spectrometer.

Results

Formation of Carotenoid Radicals ($Car^{\bullet+}$ and $\#Car^{\bullet}$) in the Model System Cu(II)-MCM-41

According to recent studies,[17,18] under photo-irradiation, $Car^{\bullet+}$ loses a proton from the methyl groups attached to the 5(5')-, 9(9')-, and 13(13')-positions, and from the 4(4')-position to produce $\#Car^{\bullet}(5)$, $\#Car^{\bullet}(9)$, $\#Car^{\bullet}(13)$ and $\#Car^{\bullet}(4)$ neutral radicals, shown in Chart 1. DFT calculations in the gas phase indicate that $\#Car^{\bullet}(4)$ is the lowest energy structure with the longest conjugation chain, as indicated by the unpaired spin density distribution in Chart 1. The calculated energy differences between the neutral radicals formed by proton loss from the methyl group and $\#Car^{\bullet}(4)$ (Table 1) are 5, 10, 12 kcal/mol for $\#Car^{\bullet}(5)$, $\#Car^{\bullet}(9)$ and $\#Car^{\bullet}(13)$, respectively.[18] Deprotonation of $Car^{\bullet+}$ occurs in the presence of water, but not in its absence.[38] Because the sample was prepared under light in humid air, the proposed reactions are as below:

$$Car + Cu^{2+} \rightarrow Car^{\bullet+} + Cu^{+} \quad (1)$$

$$Car^{\bullet+} + H_2O \rightarrow \#Car^{\bullet} + H_3O^{+} \quad (2)$$

Reaction 1 was confirmed by our previous study, which showed that Car coordinates to Cu^{2+} when it diffuses into activated Cu(II)-MCM-41 and that there is reversible electron transfer between Car and Cu^{2+}.[22] Reaction 2 indicates that, in the presence of water, $Car^{\bullet+}$ deprotonates to form $\#Car^{\bullet}$. Reactions 1 and/or 2 may also be promoted by light. However, it is very challenging to prepare the sample in complete darkness, and, therefore, it is difficult to determine the role of light for reactions 1 and 2.

For reaction 1 to occur, Cu(II)-MCM-41 must be activated to remove water. If water is coordinated with Cu^{2+} in Cu(II)-MCM-41, Car cannot coordinate with Cu^{2+}, and reaction 1 does not occur. This is proven by the fact that there is no color change after Car diffuses into fresh, water-containing Cu(II)-MCM-41. Additionally, there is no color change if the activated Cu(II)-MCM-41 is exposed to humid air for a period of 30 minutes or more before adding Car.

ENDOR Measurements of Carotenoid Radicals ($Car^{\bullet+}$ and $\#Car^{\bullet}$) in the Model System Cu(II)-MCM-41

The experimental pulsed Mims ENDOR spectrum of the blue-green mixture of Car radicals imbedded in activated Cu-MCM-41 recorded at 20 K is shown in Figure 1a. In Figure 1b, the spectrum is simulated using the DFT-derived isotropic and anisotropic coupling constants for $Car^{\bullet+}$. However, better agreement between experiment and simulation is obtained by including in the simulation the DFT-derived couplings for $\#Car^{\bullet}(4)$, $\#Car^{\bullet}(5)$, $\#Car^{\bullet}(9)$ and $\#Car^{\bullet}(13)$ in a 1:1:1:1 ratio in addition to those of $Car^{\bullet+}$, as seen in Figure 1c. Simulations including other ratios did not result in a significant improvement to the fit. However, ENDOR is a nonlinear spectroscopy that depends on relaxation, and is thus not sensitive to variations in the radical concentration, preventing quantification of the concentration of different $\#Car^{\bullet}$. ENDOR reveals the presence of $\#Car^{\bullet}$ in the sample based on peaks in the B-B' region, where the fit of simulations improves by including the DFT-derived couplings of $\#Car^{\bullet}$, and based on peaks in the C-C' region, which can only be generated in simulations only by including the DFT-derived couplings of $\#Car^{\bullet}$, as in Figure 1c. It has been found that all neutral radical species are generated in approximately equal amounts in the MCM-41 matrix,[17–19,28] an observation that is reinforced in the current work.

From Table 1, which shows the isotropic coupling constants for the radicals, one can note that the rapidly rotating isotropic methyl protons of $Car^{\bullet+}$ contribute to the A-A' regions due to isotropic couplings less than 8 MHz, while the methyl protons of $\#Car^{\bullet}$ radicals contribute to the B-B' regions due to isotropic couplings as large as 16 MHz. Peaks in the B-B' regions in Figure 1b are caused by the anisotropic coupling constants of $Car^{\bullet+}$. However, adding the isotropic couplings of $\#Car^{\bullet}$ radicals to this region (as seen in Figure 1c) greatly improves the spectrum. Also, the broad lines in the C-C' region are a result of the large anisotropic coupling constants for $\#Car^{\bullet}$ radicals, in particular those of $\#Car^{\bullet}(9)$ and $\#Car^{\bullet}(13)$. Although it is partially obscured by a baseline shift, the partner to the peak centered at 25 MHz is present in the experimental spectrum at about 5 MHz. This peak centered at 5 MHz can only be reproduced when neutral radicals in the ratio of 1:1:1:1 are included in the simulation in addition to $Car^{\bullet+}$, as in Figure 1c. The anisotropic couplings for all radicals are listed in the supporting information section. In the experimental spectrum, shown in Figure 1a, the peaks around 15 MHz are due to the matrix protons and are not considered in the spectral simulations. The peak around 3 MHz, due to ^{29}Si from the silica matrix, is also not considered in the simulation.

Visible/Near-IR Absorption Peaks of β-carotene Neutral Radicals (#Car•) in Cu(II)-MCM-41

The visible/near-IR spectrum of the Car radicals formed in Cu(II)-MCM-41 shows that the complex of Car and Cu(II)-MCM-41 displays absorption peaks at 525, 715 and 750 nm, as seen in Figure 2. The peak at 715 nm is broad and asymmetric, with a shoulder at 680 nm, probably due to the overlap of two absorption peaks. The absorption peak at 525 nm, due to unreacted Car, is also broad. The absorption peak at 950 nm, due to $Car^{\bullet+}$ which is produced in MCM-41 matrix,[39] is not detected due to the fact that $Car^{\bullet+}$ was deliberately, completely hydrolyzed under the sample preparation conditions, which did not involve the 77 K illumination that was used for the ENDOR samples.

To assign the detected absorption peaks, the maximum absorption wavelengths of $Car^{\bullet+}$, $\#Car^{\bullet}(4)$, $\#Car^{\bullet}(5)$, $\#Car^{\bullet}(9)$ and $\#Car^{\bullet}(13)$ in the gas phase were calculated using the TD-DFT method. The DFT-calculation results show that the maximum absorption wavelength of $Car^{\bullet+}$ of 829 nm is 224 nm higher than that of $\#Car^{\bullet}(4)$ listed in Table 2. If the TD-DFT calculations are scaled by 0.4 eV to accommodate for the solvent effect and the errors in the DFT calculations for $\#Car^{\bullet}$, then the estimated absorption for $\#Car^{\bullet}$ would occur around 752, 715, 675 and 536 nm. Based on the calculations, the absorption peak at 750 nm is assigned to $\#Car^{\bullet}(4)$, the broad absorption peak at 715 nm is assigned to $\#Car^{\bullet}(5)$, and its shoulder at 675 nm is assigned to $\#Car^{\bullet}(9)$. The absorption peak of $\#Car^{\bullet}(13)$ appears as a shoulder of the peak near 500 nm, which is due to unreacted Car.

The assignment of the absorption peak at 750 nm to $\#Car^{\bullet}(4)$ is additionally supported by the fact that the maximum absorption wavelength difference between this peak and that of $Car^{\bullet+}$ in the MCM-41 matrix[39] of 200 nm is similar to the calculated difference of 224 nm between $\#Car^{\bullet}(4)$ and $Car^{\bullet+}$ in the gas phase. The differences between the maximum absorption wavelengths found experimentally and those calculated by the TD-DFT method are typical of previous reports, as well as those found for ZINDO/S calculated spectra for $Car^{\bullet+}$, Car^{2+} and Car.[11] The wavelength maximum of $Car^{\bullet+}$, with 11 conjugated double bonds, in nonpolar hexane has been experimentally shown to be 940–1070 nm. In polar methanol, the absorbance maximum is blue-shifted.[40,41] The observed wavelength maxima[7] for $Car^{\bullet+}$ in PS II of 982 and 1027 nm indicates the lipophilic surroundings for Car in PS II.

Carotenoid neutral radicals have been generated by other methods and it is informative to compare prior studies of carotenoid neutral radicals with the present work. Carotenoids are known to react with free radicals by electron transfer (eq. 3), hydrogen abstraction (eq. 4) and addition to the carotenoid (eq. 5) leading to formation of the radical cation, adducts, ion-pairs and carotenoid neutral radicals.[41] Previous work has shown that carotenoids can react with

thyil radicals and acylperoxyl radicals by addition across the polyene chain to form neutral radicals (PhS-Car$^{\bullet}$ and Acyl-Car-OO$^{\bullet}$) that absorb in the visible region (450–550 nm).[42,43] It has also been reported that canthaxanthin and astaxanthin neutral radicals can be generated by first forming the radical anion (eq. 6) followed by protonation (eq. 7),[44] resulting in the formation of a carotenoid neutral radical with the added proton attached to the oxygen on the cyclohexene ring, and a conjugation length similar to that of the original carotenoid. Consistent with this extent of conjugation, the neutral radical has an optical absorbance at ~550 nm. In both of these prior studies, pulse radiolysis was used to generate the carotenoid neutral radicals and they were detected spectrophotometrically on the microsecond to millisecond timescale without independent measurement of the species to confirm the structure of the radicals observed. The possibility of adducts, carotenoid neutral radicals and ion-pairs has been discussed.[45]

$$\mathrm{Car+ROO^{\bullet} \rightarrow Car^{\bullet+}+ROO^{-}} \quad (3)$$

$$\mathrm{Car+ROO^{\bullet} \rightarrow Car^{\bullet}+ROOH} \quad (4)$$

$$\mathrm{Car+ROO^{\bullet} \rightarrow [ROO-Car]^{\bullet}} \quad (5)$$

$$\mathrm{Car+le^{-} \rightarrow CarO^{-\bullet}} \quad (6)$$

$$\mathrm{CarO^{-\bullet}+H^{+} \rightarrow CarOH^{\bullet}} \quad (7)$$

The #Car$^{\bullet}$ reported in the current study, having optical absorbances from 535 to 750 nm, were prepared in an MCM-41 solid matrix. EPR and UV/visible studies have established that radicals are stable in this matrix over days to weeks.[46] The structure of #Car$^{\bullet}$ in the current study is different from the structure of neutral radicals in other studies in that Car$^{\bullet+}$ is first formed by electron transfer to the Cu^{2+} of the MCM-41 matrix (eq. 1), and subsequent UV photolysis of the solid matrix containing Car$^{\bullet+}$ causes the loss of protons from Car$^{\bullet+}$ (eq. 2), forming a mixture of #Car$^{\bullet}$ by proton loss at 4(4') methylene (750 nm) and 5(5') (715 nm), 9(9') (675 nm) and 13(13') (535 nm) methyl groups. We have used UV/visible and ENDOR spectroscopies in conjunction with DFT calculations to identify and characterize the species radicals reported here.

Besides lacking an electron and a proton from the original carotenoid molecule as well as the oxygen substituents, the extent of conjugation is much longer for #Car$^{\bullet}$(4) and #Car$^{\bullet}$(5) than for neutral radicals formed by protonating the carotenoid anions,[44] consistent with the assigned wavelengths of 750 nm and 715 nm. Using the particle in a box as a model shows that the longer the conjugation length of the carotenoid, the longer the observed maximum of the absorption wavelength. The unpaired spin density distribution of the neutral radicals calculated by DFT is reported for Car[17,27] and other related carotenoids.[18,19]

Because Car$^{\bullet+}$ is easily deprotonated in Cu(II)-MCM-41, it is interesting to consider the possibility of its deprotonation in PS II.

Near-IR Peak at 750 nm in PS II Samples

When PS II samples are illuminated at low temperature, a charge separation occurs involving reduction of Q_A and oxidation of one of the secondary Car or Chl electron donors. In the near-IR, peaks develop around 990 nm, due to $Car^{\bullet+}$, and around 820 nm, due to $Chl^{\bullet+}$, as seen in Figure 3.[1–10,47] Recent studies also showed an absorption peak at 750 nm, the intensity of which increased with the increase of the irradiation time as more $Car^{\bullet+}$ and $Chl^{\bullet+}$ were produced, and decreased when $Car^{\bullet+}$ and $Chl^{\bullet+}$ decayed in the dark by charge recombination, [7] indicating that the species with the absorption peak at 750 nm is associated with the secondary electron-transfer pathways of PS II.

PS II core complexes from mutant strains have been isolated, which contain approximately the same number of chlorophylls and carotenoids as the wild type (WT) but that replace Car with β-zeacarotene.[48] One test of the assignment of the 750 nm peak to $\#Car^{\bullet}$ in WT PS II samples is to examine the near-IR peaks of the mutant. Low-temperature photo-irradiation of the mutant PS II core complexes generates near-IR peaks corresponding to $Chl^{\bullet+}$ and a near-IR peak corresponding to β-zeacarotene$^{\bullet+}$, rather than the peak corresponding to $Car^{\bullet+}$ that is generated in WT samples. β-Zeacarotene, which has two fewer conjugated double bonds than Car, is more difficult to oxidize. Therefore, the relative yield of $Chl^{\bullet+}$ to $Car^{\bullet+}$ is higher in the mutant. [48] If the 750 nm peak in WT samples were related to $Chl^{\bullet+}$, its yield would also be expected to increase. Conversely, following Gaussian deconvolution of spectra normalized to the same yield of carotenoid radical cations, it is found that the yield of the 750 nm peak in the mutant samples is approximately 60% of WT (data not shown). This behavior is inconsistent with $Chl^{\bullet+}$, but consistent with $\#Car^{\bullet}$. Interestingly, the wavelength maximum of the 750 nm peak does not shift in the mutant samples, while the absorbance maximum of the carotenoid radical cation shifts from 984 nm in the WT samples ($Car^{\bullet+}$) to 898 nm in the mutant samples (β-zeacarotene$^{\bullet+}$).[48] It is possible that deprotonation of both $Car^{\bullet+}$ and β-zeacarotene$^{\bullet+}$ results in neutral radicals with similar conjugation lengths. This matter is currently under investigation.

Effect of pH on the Relative Intensities of Near-IR Peaks in PS II Samples

To provide further evidence that the peak at 750 nm is due to $\#Car^{\bullet}$, the near-IR absorption peaks produced in *Synechocystis* PS II core complex samples were measured over a range of different pH values, as shown in Figure 3.[47] As the pH increases, the overall protonation of the protein decreases. It is expected that deprotonation of $Car^{\bullet+}$ would be facilitated at higher pH, either due to deprotonation of an adjacent residue that can accept a proton or, more likely, due to deprotonation of residues that facilitate proton movement. Table 3 shows that the total radical yield decreases with increasing pH due to competition with electron donation from Y_D;[49] however, the relative yield of the species absorbing at 750 nm to that of the $Car^{\bullet+}$ peak at 990 nm increases with increasing pH, supporting the assignment of the absorption peak at 750 nm to $\#Car^{\bullet}$.

Electron-Transfer Pathways Allowing the Formation of $\#Car^{\bullet}$ in PS II Samples

A radical cation hole, produced by charge separation in PS II, can be trapped at cryogenic temperatures on a variety of cofactors, including two redox-active Car[6,7] and several Chl.[9] The hole equilibrates throughout PS II, "hopping" to many closely-spaced cofactors until it is trapped at a low-potential, thermodynamically-stable location.[7] In order for $\#Car^{\bullet}(4)$ formation to occur in PS II, a pathway of electron transfer from Car to $P680^{\bullet+}$ would need to exist, generating $Car^{\bullet+}$ initially before proton loss occurs. Additionally, $\#Car^{\bullet}(4)$ would be likely to form adjacent to an amino-acid residue capable of acting as a proton acceptor, promoting deprotonation of $Car^{\bullet+}$ to form $\#Car^{\bullet}(4)$. Using the 2.9 Å resolution crystal structure of Guskov et al.,[24] amino-acid residues that are both able to act as proton acceptors and that are also located adjacent to the 4(4')-positions of Car molecules were identified.

In order to select amino-acid residues for study, the distances from the 4(4')-positions of Car molecules to nearby glutamic acid, aspartic acid, lysine, arginine and histidine residues were assessed, excluding histidine residues coordinated to chlorophyll molecules. The Car molecule with the closest proximity of 4.0 Å to a potential proton-accepting amino acid, aspartic acid 232 using the notation of the 3BZ1 structure (CP43-Asp232), was selected for analysis. Shown in Figure 4 is an electron-transfer pathway, involving the shortest distances between cofactors, from the Car molecule adjacent to Asp232 to $P680^{\bullet+}$, through the redox-active Car in the D2 subunit. Due to the fact that a variety of pathways occur in PS II, trapping the photo-generated radical cation hole on one of several Chl/Car cofactors, it is likely that the pathway depicted in Figure 4, involving only short "hops", occurs in some portion of reaction centers. This pathway provide a possible explanation for the formation of $\#Car^{\bullet}(4)$ and the consequent absorbance at 750 nm in PS II samples. It should be noted that several other candidate basic amino-acid residues are also located in close proximity to the 4(4')-positions of Car molecules, including CP47-Glu41 and could provide other secondary electron-transfer pathways for generation of $\#Car^{\bullet}(4)$.

Total Radical Yield in PS II Samples

The assignment of the peak at 750 nm to $\#Car^{\bullet}$ must be factored into the calculated radical yield per PS II. In a near-IR study, after illumination at 20 K for 15 minutes at pH 6.5, $Car^{\bullet+}$ was detected in a yield of 0.37 per PS II,[4] as calculated using a previously-determined extinction coefficient for the carotenoid radical cation.[50] The total radical yield according to near-IR measurements, including $Chl^{\bullet+}$, was 0.52 per PS II.[4] The radical yields of $\#Car^{\bullet}$ from pH 6.5–8.5, as a percent of $Car^{\bullet+}$ radical yield, are shown in Table 3. The $\#Car^{\bullet}$ yield was determined by using the value of f calculated by DFT methods, assuming that the line widths of the $\#Car^{\bullet}$ peak and the $Car^{\bullet+}$ peak were comparable and that the calculated f was proportional to the extinction coefficient. Incorporating the additional yield of $\#Car^{\bullet}$ raises the total radical yield only slightly to 0.53 per PS II. This number is closer to the 0.81 per PS II measured using EPR spectroscopy,[4] and may be increased in the future by the detection of additional $\#Car^{\bullet}$ with proton loss from different positions such as $\#Car^{\bullet}(5)$, $\#Car^{\bullet}(9)$ and $\#Car^{\bullet}(13)$, which are expected to absorb at lower wavelengths that were not examined in the present study.

Possibility of Car^{2+} in PS II Samples

Prior work has shown that two charge separations in the same PS II complex cannot occur during illumination at cryogenic temperatures.[51] Therefore, it is very unlikely that double oxidation of Car to form Car^{2+} could occur in PS II samples under the same conditions. However, to exclude the possibility that the absorption peak at 750 nm is due to the β-carotene dication (Car^{2+}), the maximum absorption wavelength (λ) and oscillator strength of Car^{2+} were calculated by the TD-DFT method and compared to the calculated values of $Car^{\bullet+}$. For Car^{2+}, the calculated λ is 743 nm and f is 4.00. The calculated maximum absorption wavelength difference between Car^{2+} (743 nm) and $Car^{\bullet+}$ (829 nm) in the gas phase is 86 nm, similar to the reported difference[52] between the two species produced in CH_2Cl_2 of 74 nm. This is much smaller than the difference of 232 nm between the absorption peak at 750 nm and $Car^{\bullet+}$ peak at 982 nm in PS II samples. Therefore, we conclude that the absorption peak at 750 nm is not due to Car^{2+}.

Conclusions

The β-carotene radical cation is easily deprotonated in model systems, and the deprotonation is facilitated in the presence of a good proton acceptor such as water. Deprotonation of the β-carotene radical cation is also postulated to occur in PS II samples, explaining the origin of the previously unassigned near-IR absorption peak at 750 nm and suggesting that the extensive secondary electron-transfer pathway in PS II may also be involved in proton transfer.

Supplementary Material

Refer to Web version on PubMed Central for supplementary material.

Acknowledgments

This work was supported by U. S. Department of Energy Grants DE-FG02-86-ER-13465 (L.D.K.) and DE-FG02-05-ER-15646 (G.W.B.) and National Science Foundation Instrumentation Grants CHE-0342921 (Alabama) and CHE-0215926 (Yale).

Abbreviations

Car	β-carotene
$Car^{\bullet+}$	β-carotene radical cation
#$Car^{\bullet}$(X)	β-carotene neutral radical, where # indicates proton loss at position X
Chl	monomeric chlorophyll
$Chl^{\bullet+}$	chlorophyll radical cation
Cu(II)-MCM-41	Cu^{2+} substituted MCM-41 silicate molecular sieve
DFT	density functional theory
ENDOR	electron-nuclear double resonance
EPR	electron paramagnetic resonance
f	oscillator strength
LHC II	light-harvesting complex II of PS II
MCM-41	Mobile Crystalline Material
near-IR	near-infrared
OEC	oxygen-evolving complex
P_{680}	primary electron-donor chlorophyll of PS II
PS II	photosystem II
Q_A	bound quinone electron acceptor in PS II
TD-DFT	time-dependent DFT
WT	wild type
Y_D	redox-active tyrosine 160 of the D2 polypeptide of PS II.

References

(1). Frank HA, Brudvig GW. Biochemistry 2004;43:8607. [PubMed: 15236568]
(2). Schenck CC, Diner B, Mathis P, Satoh K. Biochim. Biophys. Acta Bioenergetics 1982;680:216.
(3). Hanley J, Deligiannakis Y, Pascal A, Rutherford AW. Biochemistry 1999;38:8189. [PubMed: 10387064]
(4). Tracewell CA, Cua A, Stewart DH, Bocian DF, Brudvig GW. Biochemistry 2001;40:193. [PubMed: 11141071]
(5). Tracewell CA, Vrettos JS, Bautista JA, Frank HA, Brudvig GW. Arch. Biochem. Biophys 2001;385:61. [PubMed: 11361027]
(6). Telfer A, Frolov D, Barber J, Robert B, Pascal A. Biochemistry 2003;42:1008. [PubMed: 12549921]
(7). Tracewell CA, Brudvig GW. Biochemistry 2003;42:9127. [PubMed: 12885246]

(8). Stewart DH, Cua A, Chisholm DA, Diner BA, Bocian DF, Brudvig GW. Biochemistry 1998;37:10040. [PubMed: 9665709]

(9). Tracewell CA, Brudvig GW. Biochemistry 2008;47:11559. [PubMed: 18850718]

(10). Stewart DH, Brudvig GW. Biochim. Biophys. Acta 1998;1367:63. [PubMed: 9784607]

(11). Jeevarajan JA, Wei CC, Jeevarajan AS, Kispert LD. J. Phys. Chem 1996;100:5637.

(12). Jeevarajan AS, Kispert LD, Chumanov G, Zhou C, Cotton TM. Chem. Phys. Lett 1996;259:515.

(13). Wei CC, Gao G, Kispert LD. J. Chem. Soc., Perkin Trans. 2 1997;2:783.

(14). Gao G, Wei CC, Jeevarajan AS, Kispert LD. J. Phys. Chem 1996;100:5362.

(15). Krawczyk S. Chem. Phys 1998;230:297.

(16). Kispert LD, Konovalova T, Gao Y. Arch. Biochem. Biophys 2004;430:49. [PubMed: 15325911]

(17). Gao Y, Focsan AL, Kispert LD, Dixon DA. J. Phys. Chem. B 2006;110:24750. [PubMed: 17134239]

(18). Lawrence J, Focsan AL, Konovalova TA, Molnar P, Deli J, Bowman MK, Kispert LD. J. Phys. Chem. B 2008;112:5449. [PubMed: 18393549]

(19). Focsan AL, K. BM, Konovalova TA, Molnár P, Deli J, Dixon DA, Kispert LD. J. Phys. Chem. B 2008;112:1806. [PubMed: 18205344]

(20). Liu Z, Yan H, Wang K, Kuang T, Zhang J, Gui L, An X, Chang W. Nature 2004;428:287. [PubMed: 15029188]

(21). Standfuss J, van Scheltinga ACT, Lamborghini M, Kühlbrant W. EMBO Journal 2005;24:919. [PubMed: 15719016]

(22). Gao Y, Konovalova TA, Lawrence JN, Smitha MA, Nunley J, Schad R, Kispert LD. J. Phys. Chem. B 2003;107:2459.

(23). Gao Y, Kispert LD, van Tol J, Brunel LC. J. Phys. Chem. B 2005;109:18289. [PubMed: 16853353]

(24). Guskov A, Kern J, Gabdulkhakov A, Broser M, Zouni A, Saenger W. Nat. Struct. Mol. Biol 2009;16:334. [PubMed: 19219048]

(25). Beck JS, Vartuli JC, Roth WJ, Leonowicz ME, Kresge CT, Schmitt KD, Chu CTW, Olson DH, Sheppard EW, McCullen SB, Higgins JB, Schlenker JL. J. Am. Chem. Soc 1992;114:10834.

(26). Piekara-Sady L, Jeevarajan AS, Kispert LD. Chem. Phys. Lett 1993;207:173.

(27). Focsan, AL. Ph.D. Dissertation. University of Alabama; 2008.

(28). Focsan AL, Molnár P, Deli J, Kispert LD. J. Phys. Chem. B 2009;113:6087. [PubMed: 19344105]

(29). Grant JL, Kramer VJ, Ding R, Kispert LD. J. Am. Chem. Soc 1988;110:2151.

(30). Khaled M, Hadjipetrou A, Kispert LD. J. Phys. Chem 1990;94:5164.

(31). Khaled M, Hadjipetrou A, Kispert LD, Allendoerfer RD. J. Phys. Chem 1991;95:2438.

(32). Frisch, MJ.; Trucks, GW.; Schlegel, HB.; Scuseria, GE.; Robb, MA.; Cheeseman, JR.; Montgomery, JA., Jr.; Vreven, T.; Kudin, KN.; Burant, JC.; Millam, JM.; Iyengar, SS.; Tomasi, J.; Barone, V.; Mennucci, B.; Cossi, M.; Scalmani, G.; Rega, N.; Petersson, GA.; Nakatsuji, H.; Hada, M.; Ehara, M.; Toyota, K.; Fukuda, R.; Hasegawa, J.; Ishida, M.; Nakajima, T.; Honda, Y.; Kitao, O.; Nakai, H.; Klene, M.; Li, X.; Knox, JE.; Hratchian, HP.; Cross, JB.; Adamo, C.; Jaramillo, J.; Gomperts, R.; Stratmann, RE.; Yazyev, O.; Austin, AJ.; Cammi, R.; Pomelli, C.; Ochterski, JW.; Ayala, PY.; Morokuma, K.; Voth, GA.; Salvador, P.; Dannenberg, JJ.; Zakrzewski, VG.; Dapprich, S.; Daniels, AD.; Strain, MC.; Farkas, O.; Malick, DK.; Rabuck, AD.; Raghavachari, K.; Foresman, JB.; Ortiz, JV.; Cui, Q.; Baboul, AG.; Clifford, S.; Cioslowski, J.; Stefanov, BB.; Liu, G.; Liashenko, A.; Piskorz, P.; Komaromi, I.; Martin, RL.; Fox, DJ.; Keith, T.; Al-Laham, MA.; Peng, CY.; Nanayakkara, A.; Challacombe, M.; Gill, PMW.; Johnson, B.; Chen, W.; Wong, MW.; Gonzalez, C.; Pople, JA. Gaussian 03, revision B.02. Gaussian, Inc.; Pittsburgh: 2003.

(33). Zhan C-G, Dixon DA. J. Mol. Spectrsc 2002;216:81.

(34). Matsuzawa N, Ishitani A, Zhan C-G, Dixon DA, Uda T. J. Fluorine Chem 2003;122:27.

(35). Hirata S, Zhan C-G, Apra E, Windus TL, Dixon DA. J. Phys. Chem. A 2003;107:10154.

(36). Matsuzawa NN, Ishitani A, Dixon DA, Uda T. J. Phys. Chem. A 2001;105:4953.

(37). Astashkin, A. SimBud/SpecLab Software. University of Arizona; http://quiz2.chem.arizona.edu/epr/epr_000006.htm

(38). Gao Y, Webb S, Kispert LD. J. Phys. Chem. B 2003;107:13237.

(39). Gao Y, Konovalova TA, Xu T, Kispert LD. J. Phys. Chem. B 2002;106:10808.

(40). Land EJ, Lafferty J, Sinclair RS, Truscott TG. J. Chem. Soc. Faraday Trans. I 1978;74:538.

(41). Edge, R.; Truscott, TG. The Photochemistry of Carotenoids. Frank, HA.; Young, AJ.; Britton, G.; Cogdell, RJ., editors. Vol. Vol. 8. Kluwer Academic Publishers; The Netherlands: 1999. p. 223

(42). El-Agamey A, McGarvey DJ. Org. Lett 2005;7:3957. [PubMed: 16119941]

(43). El-Agamey A, McGarvey DJ. Free Radical Res 2007;41:295. [PubMed: 17364958]

(44). El-Agamey A, Edge R, Navaratnam S, Land EJ, Truscott TG. Org. Lett 2006;8:4255. [PubMed: 16956200]

(45). El-Agamey A, Lowe GM, McGarvey DJ, Mortensen A, Phillip DM, Truscott TG, Young AJ. J. Arch. Biochem. Biophys 2004;430:37.

(46). Konovalova TA, Gao Y, Schad R, Kispert LD. J. Phys. Chem. B 2001;105:7459.

(47). Tracewell, CA. Ph.D. Dissertation. Yale University; 2005.

(48). Bautista JA, Tracewell CA, Schlodder E, Cunningham FX, Brudvig GW, Diner BA. J. Biol. Chem 2005;280:38839. [PubMed: 16159754]

(49). Faller P, Rutherford AW, Debus RJ. Biochemistry 2002;41:12914. [PubMed: 12390016]

(50). Tan Q, Kuciauskas D, Lin S, Stone S, Moore AL, Moore TA, Gust D. J. Phys. Chem. B 1997;101:5214.

(51). McEvoy JP, Brudvig GW. Biochemistry 2008;47:13394. [PubMed: 19053286]

(52). Gao Y, Kispert LD. J. Phys. Chem. B 2003;107:5333.

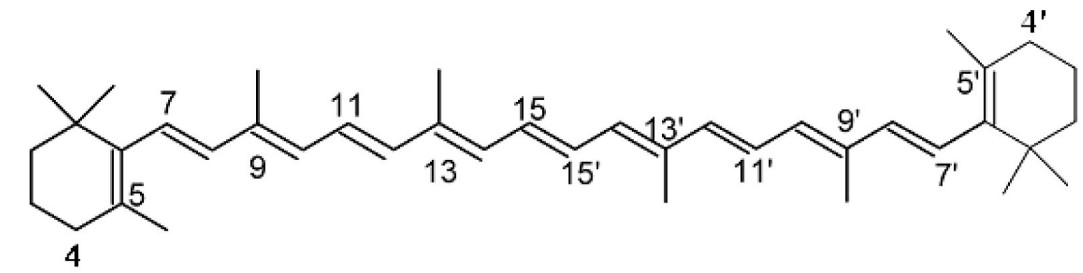

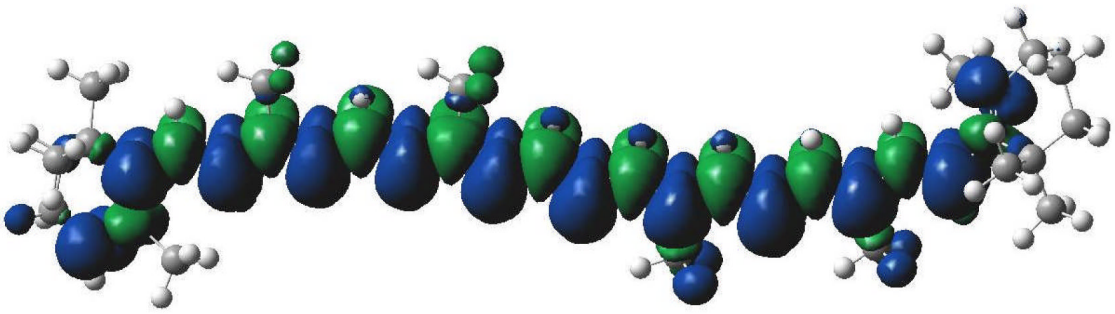

(A) $Car^{\bullet+}$

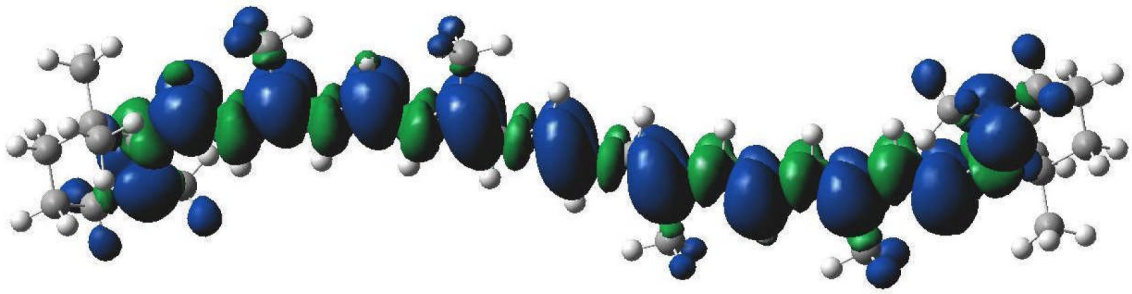

(B) $\#Car^{\bullet}(4)$

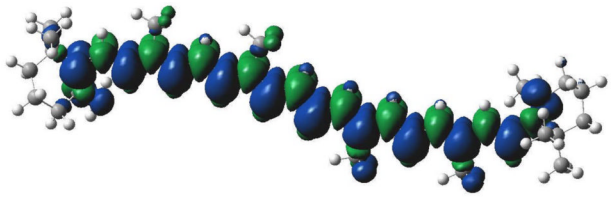

(C) #Car$^{\bullet}$(5)

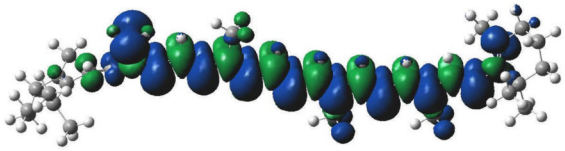

(D) #Car$^{\bullet}$(9)

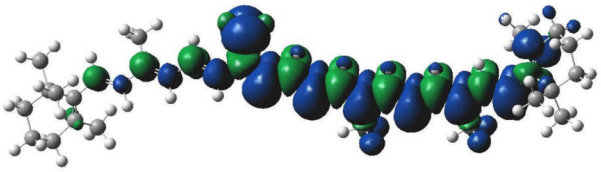

(E) #Car$^{\bullet}$(13)

Chart 1.

The structure of all-*trans* β-carotene (top) and the unpaired spin distribution from DFT calculations for: (A) β-carotene carotenoid radical (Car$^{\bullet+}$); and (B–E) carotenoid neutral radicals formed by loss of a proton from the 4(4') methylene position, and 5(5'), 9(9') and 13 (13') methyl positions of the β-carotene carotenoid radical, respectively.

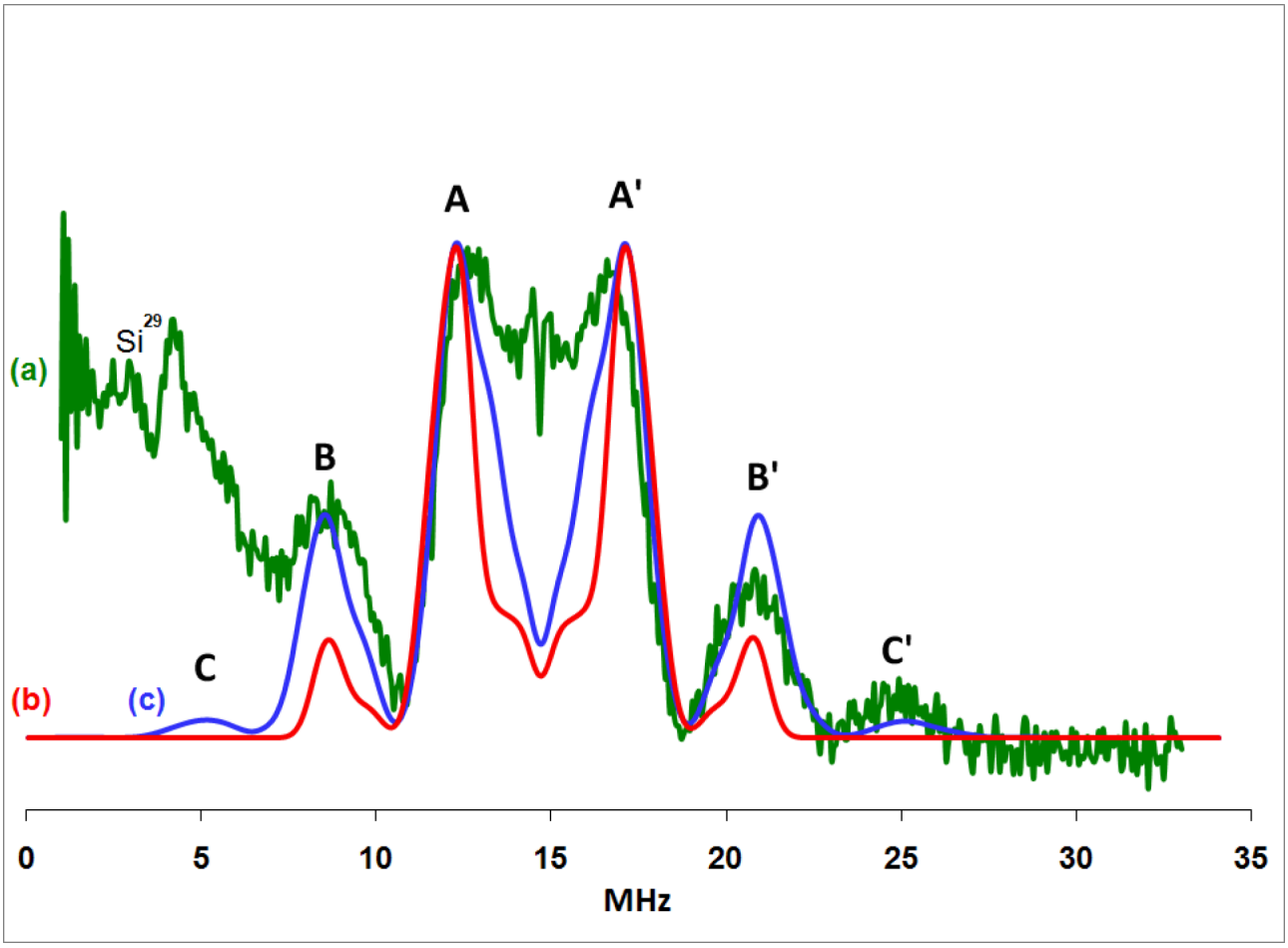

Figure 1.

Pulsed Mims ENDOR spectra of β-carotene radicals. (a) green, experimental spectrum produced in activated Cu(II)-MCM-41 after UV irradiation; ENDOR parameters: T = 20 K, *B* = 3442.9 G, ν = 9.657703 GHz, τ = 120 ns. (b) red, simulated spectrum using isotropic and anisotropic DFT-calculated couplings of $Car^{\bullet+}$ only. ENDOR lines occur at $\nu_n \pm A/2$, where ν_n is the proton frequency situated in the center of the ENDOR spectrum. (c) blue, simulated spectrum using isotropic and anisotropic DFT-calculated hyperfine couplings for $Car^{\bullet+}$, #$Car^{\bullet}$(4), #$Car^{\bullet}$(5), #$Car^{\bullet}$(9) and #$Car^{\bullet}$(13) in a 1:1:1:1:1 ratio.

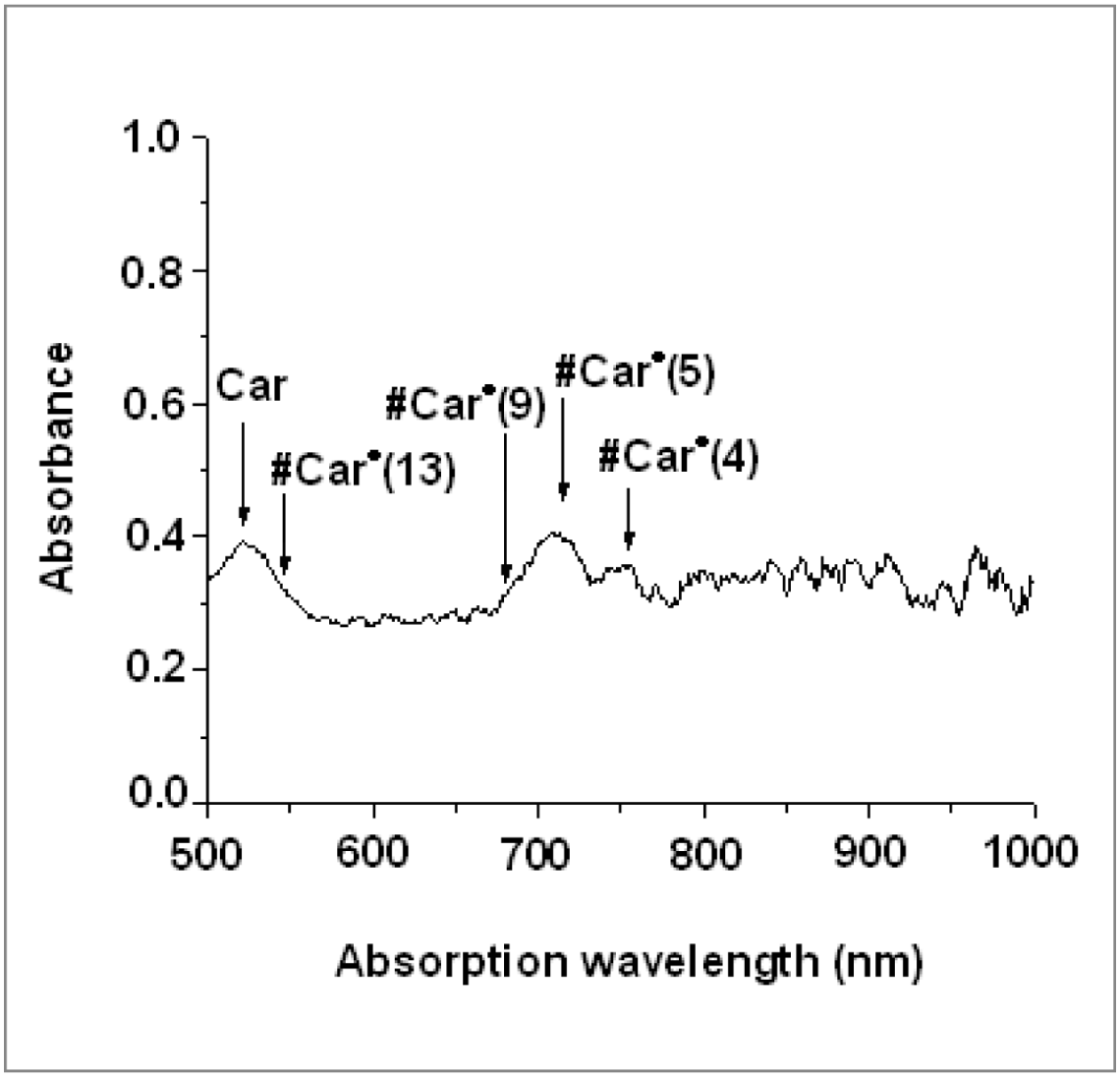

Figure 2.
Visible/near-IR spectrum of β-carotene neutral radicals produced in Cu(II)-MCM-41 in humid air under ambient fluorescent light.

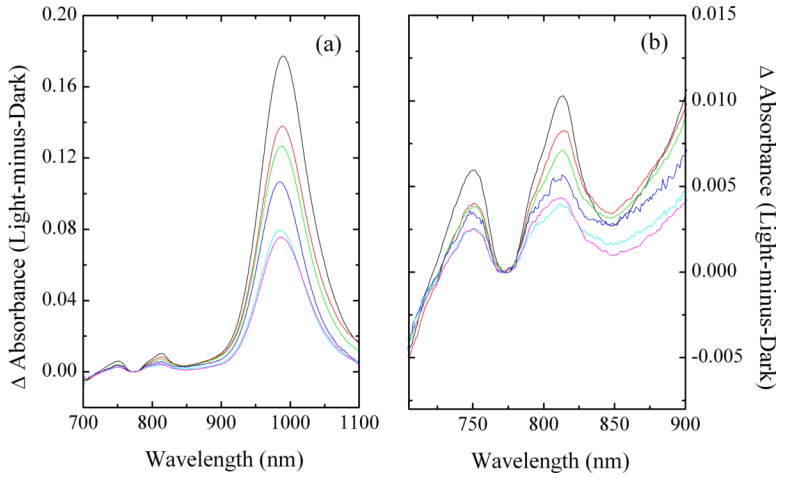

Figure 3.

Near-IR absorbance spectra of O_2-evolving *Synechocystis* PCC 6803 PS II core complexes at pH 6.0 (black), pH 6.5 (red), pH 7.0 (green), pH 7.5 (blue), pH 8.0 (cyan), and pH 8.5 (pink) illuminated by white light for 15 min at 20 K (a) from 700 – 1100 nm and (b) expanded in the 700 – 900 nm range. Chl concentration is 0.14 mg Chl/mL.

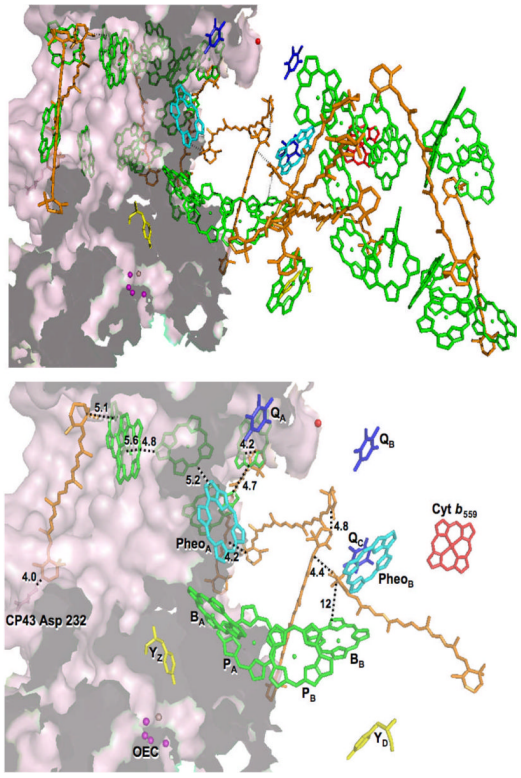

Figure 4.

Possible path of electron transfer from the Car adjacent to CP43-Asp232 (pink) to $P680^{\bullet+}$, generated from PDB code 3BZ1. Included are Chls (green), Cars (orange), Cyt b_{559} (red), the OEC (purple), pheophytins (cyan) and quinones (dark blue). The surface of CP43 is colored pale pink. The top panel shows all cofactors, while the bottom panel shows, from the same angle, only the cofactors involved in the proposed pathway as well as the central cofactors for reference. Distances (Å) between cofactors are indicated.

Table 1

Isotropic β-methyl proton hyperfine couplings (MHz) of β-carotene radicals from DFT calculations. In addition to these couplings, the anisotropic α-proton hyperfine couplings listed in Supporting Information were used to simulate the pulsed ENDOR powder spectra in Figure 1.[a]

Position	DFT Calculated A_{iso}				
	Car$^{\bullet+}$	**#Car$^{\bullet}$(4)**	**#Car$^{\bullet}$(5)**	**#Car$^{\bullet}$(9)**	**#Car$^{\bullet}$(13)**
		ΔE = 0	ΔE = 5	ΔE = 10	ΔE = 12
C1-CH$_3$	0.01 A-A′	0.43 A-A′	0.48 A-A′	−0.004 A-A′	−0.01 A-A′
	−0.04 A-A′	−0.08 A-A′	0.17 A-A′	−0.005 A-A′	−0.002 A-A′
C1′-CH$_3$	0.01 A-A′	0.05 A-A′	0.01 A-A′	0.01 A-A′	0.004 A-A′
	0.04 A-A′	−0.01 A-A′	0.03 A-A′	0.04 A-A′	0.05 A-A′
C5-CH$_3$	5.89 A-A′	−1.75 A-A′	–	−0.17 A-A′	−0.21 A-A′
C5′-CH$_3$	5.89 A-A′	2.59 A-A′	2.12 A-A′	2.48 A-A′	3.43 A-A′
C9-CH$_3$	7.05 A-A′	−5.09 A-A′	−3.12 A-A′	–	−1.14 A-A′
C9′-CH$_3$	7.05 A-A′	9.92 B-B′	8.44 B-B′	9.23 B-B′	12.03 B-B′
C13-CH$_3$	4.60 A-A′	−7.75 A-A′	5.42 A-A′	−5.32 A-A′	–
C13′-CH$_3$	4.60 A-A′	13.96 B-B′	12.48 B-B′	13.31 B-B′	15.87 B-B′

ΔE = relative energies for the neutral radicals in kcal/mol.

[a]The letters A-A′ and B-B′ indicate the peaks in Figure 1 corresponding to the couplings.

Table 2

Maximum absorption wavelengths (λ) and oscillator strengths (f) of β-carotene neutral radicals

Species	λ (nm) (gas phase) DFT prediction	f (gas phase) DFT prediction	λ (nm) observed in Cu (II)-MCM-41	λ (nm) DFT-scaled by 0.4 eV to match the observed #Car• species
#Car•(4)	605	4.0	750	752
#Car•(5)	581	3.9	715	715
#Car•(9)	543	3.1	675	675
#Car•(13)	457	1.3	535	536

Table 3

Ratio of radical yields after 15 min of illumination at 20 K over the pH range 6.5–8.5. Errors were estimated by measuring the point-to-point variations in the absorbance maximum for each pH sample ($0.5–1.2 \times 10^{-4}$ absorbance units) and propagation of error was used to estimate the error in the ratio $\#Car^{\bullet}/Car^{\bullet+}$.

pH	$\#Car^{\bullet}$ per PS II (%)	$Car^{\bullet+}$ per PS II (%)	$\#Car^{\bullet}/Car^{\bullet+}$ (%)
6.5	0.57	21	2.7 ± 0.1
7.0	0.54	19	2.8 ± 0.1
7.5	0.49	16	3.0 ± 0.1
8.0	0.36	12	3.0 ± 0.1
8.5	0.36	11	3.1 ± 0.1